Iranian Journal of Analytical Chemistry
Volume 12, Issue 2, September 2025 (129-141) Original Research Article

مجله ایرانی شیمی تجزیه
دوره ۱۲، شماره ۲، مهر ۱۴۰۴ (۱۴۱-۱۲۹)

Integrated Analytical Characterization of Mineral Nanoparticles Isolated from Baktar Hot Spring Water and Their Antibacterial Performance

Roostam Jamali Eslami[1], Mehdi Hosseini[*2]

[1]Kharazmi Exceptional Talents School, Sonqor Koliaei Education District, Songor, Kermanshah, Iran.
[2]Department of Chemistry, Faculty of Basic Sciences, Ayatollah Boroujerdi University, Boroujerd, Iran.

Received: 16 May 2025 **Accepted:** 19 July 2025
DOI: 10.30473/IJAC.2026.78061.1346

Abstract
Hot springs are natural geothermal systems enriched with dissolved minerals and nano/micro-sized particles that may contribute to their traditional therapeutic properties. In the present study, mineral nanoparticles (MNPs) were isolated for the first time from the Baktar hot spring located in western Iran, and their physicochemical characteristics as well as antibacterial activity were investigated. Structural analyses using FTIR, XRD, XRF, ICP-MS, and TGA revealed that the particles mainly consist of silicate- and metal oxide-based minerals containing high levels of SiO_2 (54.07%), Al_2O_3 (15.2%), CaO (7.19%), and Fe_2O_3 (5.45%). ICP-MS analysis also demonstrated the presence of several trace and heavy metals, including Sr (685.9 ppm), V (139 ppm), Cr (105 ppm), Zn (85 ppm), and Cu (63 ppm). XRD analysis estimated an average crystallite size of approximately 49.7 nm. The antibacterial activities of heated and unheated MNPs were evaluated against *Staphylococcus aureus* ATCC 43300 and *Pseudomonas aeruginosa* using disk diffusion and minimum inhibitory concentration (MIC) assays. The inhibition zone diameter for unheated MNPs reached 19.0 ± 0.50 mm against *P. aeruginosa*, whereas lower activity was observed against *S. aureus* (9.32 ± 0.15 mm). Both heated and unheated particles exhibited an identical minimum inhibitory concentration (MIC) of 150 µg/mL. The results suggest that naturally occurring mineral nanoparticles isolated from the Baktar hot spring possess promising antibacterial properties, supporting the potential role of geothermal mineral systems in balneotherapy and biomedical applications. This study represents the first comprehensive analytical investigation of naturally occurring mineral nanoparticles isolated from the Baktar hot spring and provides new insights into the relationship between their elemental composition, physicochemical characteristics, and antibacterial properties.

Keywords
Natural mineral nanoparticles, trace element determination, hot spring water, physicochemical characterization, antibacterial activity.

1. Introduction

A hot spring is a natural discharge of groundwater heated by geothermal energy. This process occurs when infiltrated groundwater comes into contact with geothermally heated rocks associated with magmatic activity, leading to the circulation of heated, low-density water toward the Earth's surface [1,2]. During this geothermal interaction, the chemical composition of the water undergoes significant changes, resulting in the enrichment of a wide range of dissolved ions and mineral species. These include major and trace elements such as calcium, iron, and even ultra-trace metals including gold and radium, as well as various anionic species including sulfates, chlorides, bicarbonates, and silicates [3,4].

Importantly, geothermal systems are not only reservoirs of dissolved species but also active geochemical environments that facilitate the formation of naturally occurring micro- and nano-sized mineral particles. These particles represent complex inorganic–organic assemblies characterized by high surface reactivity. Owing to their natural origin, physicochemical stability, and potentially low toxicity, these mineral nanoparticles have attracted increasing attention as environmentally compatible materials with promising applications in environmental science and biomedicine [5]. However, their precise

* Corresponding author:
M. Hosseini; E-mail(s): Hosseini.mih@gmail.com; Hosseini.mehdi@abru.ac.ir

chemical composition, structural properties, and functional behavior in natural aqueous systems remain poorly understood.

Hot springs have historically been associated with therapeutic effects and have been used for centuries as traditional remedies for various physical and dermatological conditions [6]. Classical medical practices, including those of ancient Greek medicine, recommended sulphur-rich thermal waters for treating skin disorders, joint inflammation, and muscular pain [7-10]. In addition, thermal waters have been linked to beneficial effects in the management of conditions such as arthritis, respiratory disorders, circulatory dysfunctions, and rheumatic diseases. These effects are often attributed to the presence of dissolved minerals and suspended particulate matter in geothermal fluids. Despite these long-standing empirical observations, the scientific basis underlying such therapeutic claims remains limited, particularly with respect to establishing a direct relationship between the chemical nature of suspended particles and their biological activity.

From an analytical chemistry perspective, the characterization and quantification of trace species in complex environmental matrices, such as geothermal waters, require highly sensitive and selective analytical methodologies. In recent years, modern sample preparation and preconcentration techniques, particularly microextraction-based approaches, have significantly improved trace analysis in aqueous systems. Methods such as dispersive liquid-liquid microextraction (DLLME), solid-phase microextraction (SPME), ionic liquid-based extraction systems, and magnetic solid-phase extraction (MSPE) have been widely applied for the selective isolation and enrichment of metal ions and organic analytes because of their high extraction efficiency, minimal solvent consumption, and excellent compatibility with instrumental detection techniques [11-13]. When coupled with advanced analytical platforms such as ICP-MS, XRF, and various spectroscopic methods, these strategies enable the accurate determination of trace and ultra-trace species in complex environmental samples, including natural waters and geothermal systems [14-22].

In parallel, geothermal environments are known to host diverse microbial ecosystems, including thermophilic bacteria such as *Bacillus*, *Geobacillus pallidus*, and *Anoxybacillus flavithermus*, which are capable of producing bioactive compounds, including enzymes and antimicrobial agents [23,24]. Moreover, specific ionic species present in hot spring waters, such as iodide and manganese, have been suggested to contribute to various biological activities, including anti-inflammatory effects [25]. Nevertheless, despite these findings, systematic studies investigating the role of naturally occurring mineral nanoparticles in the antibacterial activity of hot spring systems remain limited.

Based on these considerations, the present study focuses on the analytical isolation, physicochemical characterization, and antibacterial evaluation of mineral nanoparticles isolated from Baktar Hot Spring, located in the western region of Kermanshah Province, Iran. This geothermal system is well known for its traditional therapeutic applications (Fig. 1); however, its particle-level chemical and biological properties have not been thoroughly investigated. The in situ physicochemical parameters of the spring were determined as pH 7.7 and a temperature of approximately 28 °C [26–28]. The present study introduces several important novelties. First, naturally occurring mineral nanoparticles (MNPs) were isolated for the first time from Baktar hot spring water. Second, a comprehensive multi-technique analytical characterization combining FTIR, XRD, XRF, ICP-MS, and TGA was employed to establish the physicochemical, elemental, and structural properties of these naturally formed nanoparticles. Third, the antibacterial activity of both heated and unheated MNPs was systematically evaluated against representative Gram-positive and Gram-negative bacteria. Finally, this work establishes a direct relationship between the chemical composition, mineralogical characteristics, and antibacterial performance of geothermal mineral nanoparticles, providing new analytical insights into the potential biomedical significance of naturally occurring nanomaterials in geothermal systems.

Fig. 1. Geographical view of Baktar hot spring located in Kermanshah province, western Iran.

2. MATERIALS AND METHOD

2.1. Characterization of particles

DOI: 10.30473/IJAC.2026.78061.1346

The isolated mineral particles were analyzed using X-ray diffraction (XRD) to identify their crystalline structure using a Philips X'Pert MPD diffractometer (PANalytical, Netherlands) equipped with Cu Kα radiation (λ = 1.5406 Å). X-ray fluorescence (XRF) spectra were obtained using a Bruker S8 TIGER spectrometer (Bruker AXS, Germany) to determine the elemental oxide composition of the isolated mineral particles. Inductively coupled plasma mass spectrometry (ICP-MS, Agilent 7900, USA) was employed to quantify trace and heavy metal elements in the samples. Dynamic light scattering (DLS; Malvern Zetasizer Nano ZS 3600, UK) was utilized to evaluate the hydrodynamic particle size distribution of the mineral nanoparticles dispersed in an aqueous medium. Field emission scanning electron microscopy (FESEM, GENEX, USA) was employed to investigate the morphology and approximate particle size of the isolated mineral particles. Thermogravimetric analysis (TGA) was performed using a STA 449 F3 Jupiter thermal analyzer (NETZSCH, Germany) under a nitrogen atmosphere at a heating rate of 10 °C min^{-1} over the temperature range of 25-1000 °C. The particles were further characterized by Fourier-transform infrared spectroscopy (FT-IR, PerkinElmer Spectrum Two, USA) over the spectral range of 400-4000 cm^{-1} to identify the surface functional groups, chemical bonding, and the composition of the organic and inorganic constituents.

2.2. Isolation of MNPs from Baktar hot spring water

Approximately 1.0 L of hot spring water was collected directly from the main discharge point of Baktar hot spring using a clean polyethylene container. The collected sample was transported to the laboratory immediately and allowed to cool naturally to room temperature without any chemical treatment. The suspended mineral particles were separated by centrifugation at 10,000 rpm for 10 min. After centrifugation, the supernatant was carefully decanted, and the obtained precipitate was collected. The isolated mineral particles were dried in a laboratory oven at 100 °C for 3 h until constant weight was achieved. The dried powder was subsequently stored in a clean airtight glass vial at room temperature for further physicochemical characterization and antibacterial experiments.

2.3. Determination of antibacterial activity by disc diffusion test

The antibacterial activity of MNPs was evaluated against the Gram-positive Bacterium *Staphylococcus aureus* ATCC 43300 and the Gram-negative bacterium *Pseudomonas aeruginosa*. These bacterial strains were obtained from the Microbiology Laboratory, Kermanshah University of Medical Sciences, Iran. The disk diffusion method was employed to evaluate the antibacterial activity [29]. Fresh Mueller–Hinton agar (MHA) plates were prepared and sterilized by autoclaving prior to each experiment. Bacterial suspensions were adjusted to the 0.5 McFarland standard (approximately 1.5 × 108 CFU mL^{-1}) to ensure standardized inoculum density. Briefly, bacterial colonies were collected using a sterile cotton swab and suspended in sterile physiological saline until the turbidity matched the 0.5 McFarland standard. Subsequently, sterile Petri dishes containing 20 mL of MHA were inoculated by evenly swabbing the bacterial suspension over the agar surface. A 10 mL suspension of mineral nanoparticles (6 mg mL^{-1}), including both unheated particles and particles heated at 850 °C, was dispersed by sonication and subsequently filtered through a 0.20 µm membrane filter (47 mm diameter, Pall Gelman Laboratory). The nanoparticle-loaded membrane was dried in an oven for 1 h, after which 6 mm diameter disks containing approximately 300 µg of nanoparticles were prepared. The disks were then placed equidistantly on the surface of the inoculated agar plates [30]. The plates were incubated at 35 °C for 24 h, after which the diameter of the inhibition zone (DIZ) surrounding each disk was measured to the nearest 1 mm. The results are presented as the mean ± standard error of the mean (SEM) based on three independent replicates for each bacterial strain and each nanoparticle treatment.

2.4. Determination of the MIC of mineral nanoparticles

The minimum inhibitory concentration (MIC) is defined as the lowest concentration of a test material that inhibits approximately 99% of the visible growth of microorganisms and was determined using batch cultures containing varying concentrations of unheated and heated MNPs (34.5-300 µg mL^{-1}). Sterile tubes, each containing 3 mL of nutrient broth, were prepared, and the nanoparticle suspensions were sonicated for 20 min to prevent the aggregation of the MNPs. Subsequently, the tubes were inoculated with freshly prepared bacterial suspensions adjusted to the 0.5 McFarland standard (approximately 1.5 × 10^8 CFU mL^{-1}). The experiments also included a positive control consisting of nutrient broth and MNPs without bacterial inoculum and a negative control consisting of nutrient broth and bacterial inoculum without MNPs. The negative control represented the normal bacterial growth in the absence of MNPs, whereas the absorbance values obtained from the positive controls were subtracted from those of the corresponding experimental samples. All experiments were performed in

DOI: 10.30473/IJAC.2026.78061.1346

triplicate. The tubes were then incubated at 35 °C for 24 h, and the MIC was determined as the lowest concentration of MNPs that completely inhibited visible bacterial growth. Bacterial growth was further evaluated by measuring the optical density (OD) at 600 nm, where increased turbidity indicated bacterial growth and the absence of turbidity indicated growth inhibition.

2.5. Statistical analysis

All experiments were performed in triplicate, and the results are presented as the mean ± standard deviation (SD). Statistical analyses were performed using GraphPad Prism version 6.0 (GraphPad Software Inc., USA). One-way analysis of variance (ANOVA), followed by Bonferroni's post hoc multiple-comparison test, was applied to evaluate the statistical significance of differences between experimental groups, including the antibacterial activities of heated and unheated mineral nanoparticles against different bacterial strains. Differences were considered statistically significant at $P < 0.05$. The inhibition zone diameter (DIZ) and optical density (OD_{600}) values are reported as the mean ± SD of three independent experiments.

3. RESULTS AND DISCUSSION

Due to the presence of living organisms in hot springs, various biomolecules are naturally present in the spring water. These compounds can be adsorbed onto the surfaces of the MNPs dispersed in the spring water. [3,6,8-10,15] Traces of these compounds are evident in the Fourier-transform infrared (FTIR) spectra of the isolated particles. Fourier-transform infrared (FTIR) spectroscopy is a powerful analytical technique for identifying chemical bonds, functional groups, and the structural frameworks of both organic and inorganic compounds. Fig. 2 shows the FTIR spectra of the MNPs extracted from Baktar Hot Spring before and after heat treatment. The broad and intense absorption band centered at approximately 1039 cm^{-1} corresponds primarily to metal–oxygen (M–O) stretching vibrations, where the metal species may include Fe, Ca, Si, and Al. The absorption bands located at 2924, 2891, and 1434 cm^{-1} are assigned to the asymmetric/ symmetric stretching and bending (scissoring) vibrations of $–CH_2$ groups [31]. The broad absorption band at 3419 cm^{-1} is attributed to the stretching vibrations of O–H and N–H groups present in both organic and inorganic constituents. The presence of these absorption bands indicates that organic compounds are adsorbed onto the surfaces of the naturally occurring mineral particles. To confirm this assumption, the extracted MNPs were heated at 850 °C for 1 h to remove surface-associated organic compounds (heated MNPs). As observed in the FT-IR spectrum of the heat-treated sample, most absorption bands in the fingerprint region either disappeared or markedly decreased in intensity, indicating the thermal decomposition or removal of organic constituents. In contrast, the strong and broad metal–oxygen absorption band remained essentially unchanged, confirming that the inorganic mineral framework of the particles was preserved after heat treatment (Fig. 2) [32].

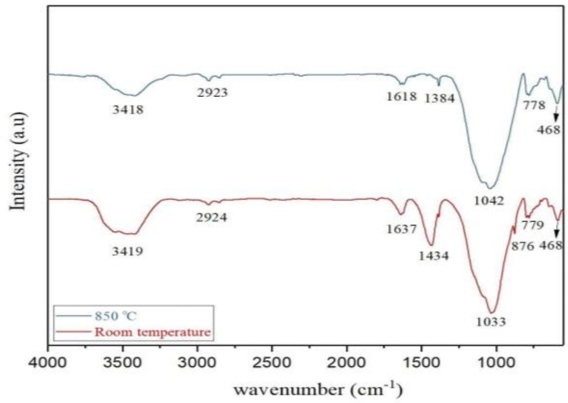

Fig. 2. FTIR spectra of particles at two different temperatures, room temperature (red line) and 850 °C (Blue line).

The thermal stability of the isolated mineral nanoparticles was evaluated by thermogravimetric analysis (TGA). Figure 3 illustrates the TGA thermogram, showing four distinct stages of weight loss as the temperature increased from 25 to 1000 °C. The first weight loss, approximately 2.5%, occurred in the temperature range of 25-280 °C and was attributed to the removal of physically adsorbed moisture and structurally bound water molecules associated with the MNPs. The second weight loss, approximately 3.5%, occurred between 280 and 650 °C and is mainly attributed to the thermal decomposition of naturally adsorbed organic matter originating from microorganisms and other biological residues present in the geothermal environment, together with the decomposition of minor volatile mineral constituents. The third weight loss, approximately 2.0%, occurred in the temperature range of 750-850 °C and can be attributed primarily to the thermal decomposition (decarbonation) of carbonate-containing mineral phases, resulting in CO_2 evolution and structural transformations within the mineral matrix. Overall, the sample exhibited a total weight loss of approximately 9% over the temperature range of 25-1000 °C, indicating that the isolated mineral nanoparticles possess good thermal stability with only a limited amount of volatile components and organic matter. These findings are consistent with the

DOI: 10.30473/IJAC.2026.78061.1346

predominantly inorganic mineral composition identified by XRD and XRF analyses [33,34].

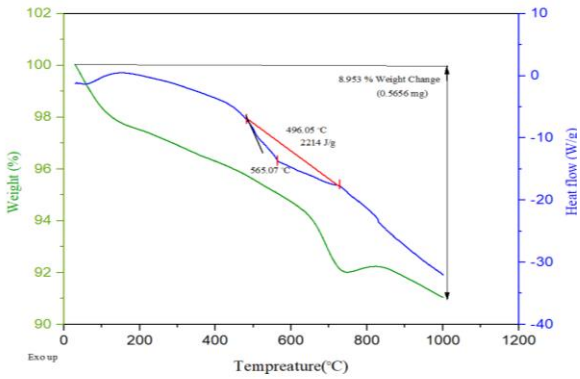

Fig. 3. TGA analysis for nanoparticles in the temperature range between 25 and 1000 °C

In Fig. 4, the XRD patterns of the MNPs exhibit diffraction peaks at 2θ ≈ 12–52°, confirming the crystalline nature of the mineral nano-/microparticles present in the hot spring sample. The narrow diffraction peaks observed at 2θ ≈ 13.7°, 15.7°, 22.03°, 23.6°, 27.8°, and 28.04° are mainly attributed to aluminosilicate mineral phases with the general composition of $(Na,Ca)(Si,Al)_4O_8$. In addition, the diffraction signals appearing at 2θ ≈ 22.03°, 27.8°, and 28.04° are assigned to $NaAlSi_3O_8$-related crystalline structures. The detected diffraction peaks also indicate the presence of iron oxide (Fe_2O_3) and silica (SiO_2) phases in the isolated particles.

The relatively sharp and intense peaks suggest a moderately crystalline and well-ordered mineral structure in the prepared sample. Furthermore, the coexistence of silicate and iron oxide phases reflects the complex geochemical composition of the geothermal environment from which the particles originated. The average crystallite size, calculated using the Debye–Scherrer equation, was approximately 49.7 nm, indicating the nanoscale nature of a considerable fraction of the isolated mineral particles [35-38]. The nanoscale dimensions of these particles can significantly increase their specific surface area and surface reactivity, which may contribute to the observed antibacterial activity. Moreover, the presence of multiple crystalline mineral phases suggests that the biological performance of the MNPs may arise from synergistic interactions between the silicate matrix and transition-metal-containing compounds. These findings are in good agreement with the XRF and ICP-MS analyses, which confirmed the abundance of silicon, aluminum, calcium, and iron-rich phases in the sample [39,40].

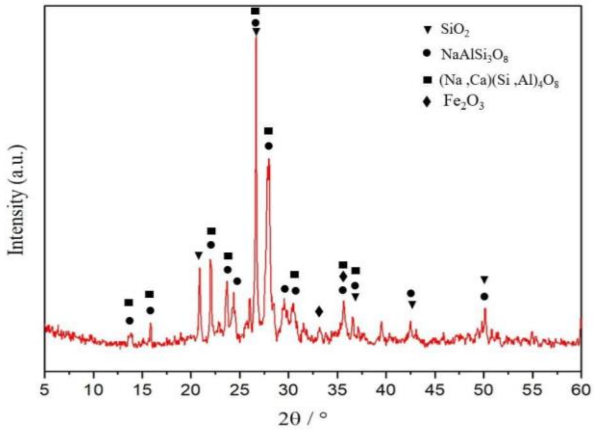

Fig. 4. XRD pattern of nanoparticles show peaks at 2θ ≈ 12-52°.

X-ray fluorescence (XRF) spectroscopy is one of the most widely used analytical techniques in both industrial and academic research. XRF is an elemental analysis technique used to determine the concentrations of the major mineral oxides and elemental constituents present in a sample. The results of the XRF analysis are presented in Table 1. The analysis revealed that SiO_2, Al_2O_3, and CaO were the predominant constituents of the MNPs isolated from Baktar Hot Spring [41].

Table 1. The main elements in the sample by XRF method.

Element	SiO_2	Al_2O_3	LOI	CaO	Fe_2O_3	Na_2O	MgO	K_2O	SO_3	TiO_2	P_2O_5	MnO	BaO	Cr_2O_3
Amounts %	54.07	15.2	8.47	7.19	5.45	3.66	2	1.79	1.15	0.67	0.13	0.07	0.06	0.01

The ICP-MS analysis was used to determine the concentrations of trace elements present at low levels in the sample. The results showed that elements such as Sr, V, Cr, Zn, and Cu were detected at concentrations exceeding 50 ppm (Table 2). These data clearly indicate the presence of heavy metals and metalloids in the isolated MNPs [42,43].

DOI: 10.30473/IJAC.2026.78061.1346

Table 2. The amount of elements in the nanoparticles by ICP method in ppm.

Element	Amount (ppm)
Sr	685.9
V	139
Cr	105
Zr	100
Zn	85
Cu	63
Li	46
W	45.6
Rb	31
Ce	23
Ni	23
Y	20.7
Co	19.7
Sc	16.4
La	14
Nd	13
As	8.7
Nb	5.3
Pb	5
Pr	3.17
Th	2.85
Hf	2.82
Cs	2.8
Dy	2.63
Sm	2.33
Yb	2.3
Mo	2
Eu	1.35
Er	1.22
Gd	1.1
Be	1
Sn	0.8
U	0.8
Ta	0.63
Ag	0.6
Sb	0.5
Tb	0.46
Te	0.33
Lu	0.32
Cd	0.3
Tm	0.27
Tl	0.16
In	<0.5
Se	<0.5
Bi	<0.1

FESEM images of the isolated mineral particles obtained from Baktar hot spring are presented in Fig. 5. The micrographs reveal that the collected material consists of irregularly shaped mineral aggregates composed of numerous fine particles with heterogeneous morphology. At low magnification (Fig. 5a), relatively large agglomerated mineral clusters with rough and compact surfaces are observed, indicating that the naturally occurring particles tend to aggregate during precipitation and drying. Higher-magnification images (Fig. 5b-d) clearly demonstrate that these aggregates are constructed from densely packed nano-sized primary particles together with a limited fraction of larger micro-sized particles. The primary particles exhibit predominantly plate-like, flaky, and irregular morphologies, which are characteristic of naturally occurring aluminosilicate and silica-rich minerals. The FESEM observations confirm that a considerable proportion of the isolated particles possess nanoscale dimensions, although particle agglomeration makes direct measurement of individual nanoparticles difficult. Such aggregation is commonly observed in naturally occurring mineral nanoparticles owing to their high surface energy and strong interparticle interactions during drying. Therefore, the particle sizes observed by FESEM are generally larger than the crystallite size estimated from XRD analysis. The XRD results yielded an average crystallite size of approximately 49.7 nm using the Debye-Scherrer equation, which is in good agreement with the FESEM observations showing that the mineral aggregates are composed of nanoscale crystalline domains. It should be noted that the crystallite size determined by XRD corresponds to coherent crystalline domains rather than the overall particle size visualized by FESEM. Consequently, the apparent discrepancy between the aggregated particle morphology observed in FESEM and the smaller crystallite size calculated from XRD is expected and reflects the polycrystalline nature of the isolated mineral particles. The irregular plate-like morphology observed in Fig. 5 is also consistent with the mineralogical composition determined by XRD, which identified crystalline aluminosilicate ($(Na,Ca)(Si,Al)_4O_8$and $NaAlSi_3O_8$), silica (SiO_2), and iron oxide (Fe_2O_3) phases. Such layered and angular morphologies are frequently reported for naturally formed aluminosilicate minerals generated in geothermal environments. Furthermore, the coexistence of silicate matrices with iron-containing mineral phases agrees well with the XRF and ICP-MS analyses, confirming that silicon, aluminum, calcium, and iron are the dominant constituents of the isolated particles. The nanoscale crystalline domains together with the rough and highly aggregated surface morphology are expected to provide a relatively high specific surface area and abundant active surface sites. These structural characteristics may facilitate interactions between the mineral particles and bacterial cell membranes, thereby contributing to the antibacterial activity observed for the isolated mineral nanoparticles.

DOI: 10.30473/IJAC.2026.78061.1346

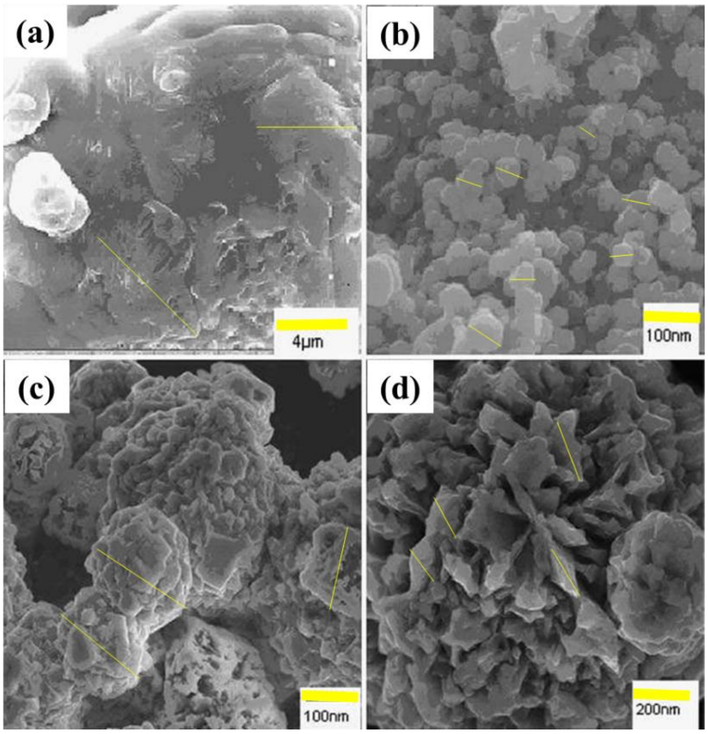

Fig. 5. FESEM micrographs of the isolated mineral nanoparticles (MNPs) from Baktar hot spring recorded at different magnifications.

The particle size distribution of the isolated mineral nanoparticles (MNPs) was further investigated by dynamic light scattering (DLS), and the obtained profile is presented in Fig. 6. The DLS spectrum exhibits a bimodal particle size distribution with a minor peak centered at approximately 75-90 nm and a dominant peak located at approximately 240-270 nm. The smaller peak is attributed to individually dispersed nanosized mineral particles, whereas the larger peak corresponds to the hydrodynamic diameter of particle aggregates formed in aqueous suspension. The broad and intense peak observed at higher particle diameters indicates that the naturally occurring mineral nanoparticles possess a pronounced tendency to agglomerate because of their high surface energy and interparticle interactions. Such aggregation behavior is commonly observed for naturally occurring silicate- and metal oxide-based nanoparticles dispersed in aqueous media. It should be noted that DLS measures the hydrodynamic diameter of particles rather than the actual crystallite size; therefore, larger particle sizes are generally expected owing to hydration effects and particle aggregation in suspension. The presence of a minor nanosized population together with a dominant agglomerated fraction indicates that the isolated mineral particles consist of nanoscale primary particles that partially aggregate after dispersion. These results provide further evidence for the heterogeneous nature of the isolated mineral nanoparticles and are in good agreement with the morphological observations obtained from FESEM as well as the crystallite size estimated by XRD analysis.

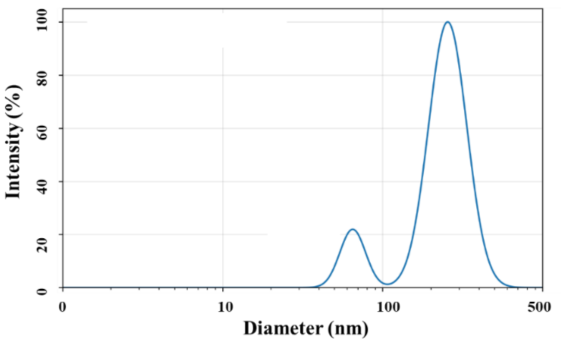

Fig. 6. Dynamic light scattering (DLS) analysis of mineral nanoparticles isolated from Baktar hot spring, illustrating the hydrodynamic particle size distribution and aggregation behavior of the dispersed mineral particles.

3.1. Antibacterial activity of MNPs against S. aureus and P. aeruginosa

After characterization of the nanoparticles isolated from the hot spring, the antibacterial properties of these MNPs were investigated. Furthermore, due to the presence of organic compounds on the surface of the MNPs, the effect of these compounds on the antibacterial properties of the

DOI: 10.30473/IJAC.2026.78061.1346

MNPs was also examined. For this purpose, the MNPs were categorized into two groups [44]. One group of MNPs was heated to 850 °C to remove the organic compounds adsorbed onto their surface (heated MNPs), whereas the other group was collected directly from Baktar Hot Spring without any thermal treatment (unheated MNPs), and their antibacterial properties were subsequently evaluated. The antibacterial activities of the unheated and heated MNPs were compared against *S. aureus* ATCC 43300 and *P. aeruginosa* using the inhibition zone diameter (DIZ) determined by the disk diffusion assay. The DIZ reflects the degree of bacterial susceptibility to the tested nanoparticles [45]. The bacterial strains that were more susceptible to the MNPs exhibited larger DIZ values, whereas less susceptible strains exhibited smaller inhibition zones. The DIZ was influenced by the type of microorganism. Specifically, *P. aeruginosa* exhibited significantly larger inhibition zones than *S. aureus* for both heated and unheated MNPs. The DIZ values obtained for *P. aeruginosa* were approximately 45–50% greater than those observed for *S. aureus*. However, for both *S. aureus* and *P. aeruginosa*, the antibacterial activities of the heated MNP-impregnated disks were comparable to those of the unheated MNP-impregnated disks. Since the DIZ was measured on agar plates using a ruler with a resolution of 1 mm, minor measurement errors may have occurred; however, this method clearly demonstrates the antibacterial potential of the MNPs against different bacterial strains (Fig. 7 and Table 3) [46].

Table 3. The DIZ surrounding MNPs impregnated disks (6 mm diameter) in presence of various microorganisms.

MNP IDs	S.aureus	P. aeruginosa
	DIZ (mm ± SEM)	
Unheated MNPs	9.32 ±0.15	19 ± 0.50
Heated MNPS	9.16 ±0.20	17 ± 0.35

DIZ = diameter of inhibition zone, MNPs = mineral nanoparticles, SEM = standard error mean

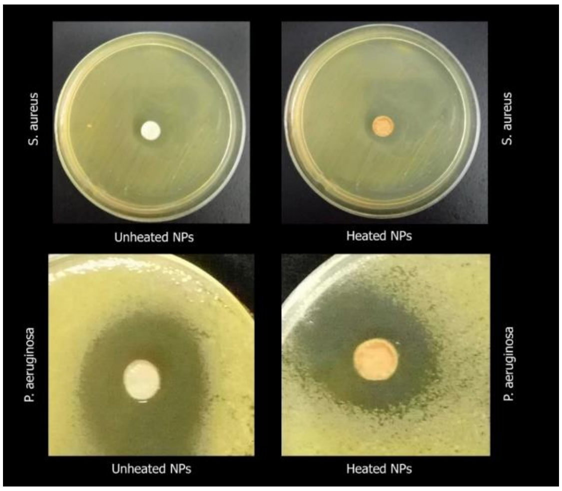

Fig. 7. Disk diffusion assay demonstrating the antibacterial activity of heated and unheated mineral nanoparticles (MNPs) against S. aureus ATCC 43300 and P. aeruginosa.

The absorbance measured at 600 nm, which reflects the antibacterial activity of MNPs dispersed in batch cultures, is presented in Table 6. As the concentration of MNPs increased to the MIC for the respective bacterial strains, no bacterial growth was observed in the test tubes. The bactericidal effect of the nanoparticles is dependent on both the initial bacterial concentration and the nanoparticle concentration. In this study, the initial bacterial concentration was maintained at approximately 1.5×10^8 CFU/mL (0.5 McFarland standard), irrespective of the MNP concentration or microbial strain. Consistent with the disk diffusion assay results, the batch culture experiments also demonstrated comparable antibacterial activities for both heated and unheated MNPs against the tested bacterial strains. The MIC values determined for both heated and unheated MNPs were 150 µg/mL against both *S. aureus* and *P. aeruginosa*.

Table 6. Absorbance (at 600 nm) for turbidity as growth in presence of varying concentration of MNPs for *S. aureus* and *P.aeruginosa.*

MNPs concentration (µg/mL)	MNPs ID	*S. aureus* OD±SD (µg/mL)	*P. aeruginosa* MIC±SD (µg/mL)
34.5	Unheated	1.2±0.1	1.2±0.1
	Heated	1.2±0.1	1.2±0.1
	Unheated	1.2±0.1	1±0.15
75	Heated	1.2±0.1	1±0.15
	Unheated	0.04±0.02	0.05±0.03
150	Heated	0.04±0.02	0.05±0.03
	Unheated	0.04±0.02	0.05±0.03
300	Heated	0.04±0.02	0.05±0.03
NC		1.2±0.1	1.3±0.1

DOI: 10.30473/IJAC.2026.78061.1346

MNPs = mineral nanoparticles, SD = standard deviation
The test tubes were monitored by measuring OD at 600 nm for turbidity as growth.

The antibacterial activity of MNPs may be due to the presence of elements such as aluminum, iron, strontium, vanadium, copper, phosphorus, calcium, sulfur, bicarbonate, etc. [24,25,47]. Heavy metals, when present at low concentrations, are essential for the cellular activities of microorganisms; however, at elevated concentrations, they become toxic to bacteria, thereby altering their morphology, growth, and metabolic activity. For example, copper, the first antimicrobial metal recognized by the U.S. Environmental Protection Agency (EPA), was reported to inactivate 99.9% of bacteria within only 2 h [48]. Londoño et al. demonstrated that aluminum-containing clay minerals exhibit antimicrobial activity against human pathogens [49]. Similarly, iron nanoparticles have been reported to inhibit the growth of clinically relevant bacteria, including *Escherichia coli* (Gram-negative) and *Staphylococcus aureus* (Gram-positive). Furthermore, Anastasiou et al. developed a strontium-decorated biomaterial scaffold that exhibited excellent antimicrobial activity together with regenerative potential [50]. Collectively, these findings demonstrate that the MNPs isolated from Baktar Hot Spring possess promising antibacterial properties and may contribute to the therapeutic efficacy of balneotherapy.

4. Conclusions

In this study, mineral nanoparticles naturally present in the water of the Baktar hot spring were successfully isolated and comprehensively characterized for the first time. Structural and compositional analyses confirmed that the extracted particles consisted predominantly of silicate- and metal oxide-based mineral phases enriched with various metallic and semi-metallic elements, including Fe, Sr, V, Cu, Zn, and Cr. FTIR and TGA analyses further demonstrated the coexistence of inorganic mineral structures with adsorbed organic compounds originating from the geothermal environment. Antibacterial evaluation demonstrated that both heated and unheated MNPs exhibited inhibitory activity against both Gram-positive and Gram-negative bacteria, with a stronger effect observed against *P. aeruginosa*. The similar antibacterial behavior of heated and unheated particles suggests that the antimicrobial activity is primarily associated with the mineral composition and metallic constituents of the nanoparticles rather than with the adsorbed organic materials. The observed MIC values and inhibition zone diameters further indicate that these naturally occurring mineral particles may serve as effective antimicrobial agents even without additional chemical modification. Overall, the findings of this study provide scientific support for the traditional therapeutic claims associated with the Baktar hot spring and highlight the possible contribution of naturally occurring mineral nanoparticles to the therapeutic effects of balneotherapy. Moreover, this study provides a new perspective for exploring geothermal springs as natural reservoirs of functional mineral nanomaterials with potential biomedical and environmental applications. Nevertheless, further investigations, including cytotoxicity assessment, studies on the antibacterial mechanism, and evaluation against a broader range of microbial species, are necessary before practical therapeutic applications can be fully established.

Acknowledgements
Research councils of Biosensor and Energy Research Center, Ayatollah Boroujerdi University are acknowledged for financial support of this work.

Disclosure statement
No potential conflict of interest was reported by the author.

Competing interests
The author declares no competing interests.

References

[1] E. Banse, M. Mikolajczak, M. Bayot, A.L. Lenoir, P. de Timary, Medical culture and its association with health outcomes in physicians: A cross-sectional study. *J. Affect. Disord. Rep.*, 23 (2026) 101018. https://doi.org/10.1016/j.jadr.2025.101018.
[2] C. Protano, M. Vitali, A. De Giorgi, D. Marotta, S. Crucianelli and M. Fontana, Balneotherapy using thermal mineral water baths and dermatological diseases: a systematic review. *Int. J. Biomet.*, 68 (2024) 1005-1013. https://doi.org/10.1007/s00484-024-02649-x.
[3] D.A. Torres-Ceron, C.D. Acosta-Medina and E. Restrepo-Parra, Geothermal and mineralogic analysis of hot springs in the Puracé-La Mina sector in Cauca, Colombia. *Geofluids*, 2019 (2019) 191454,. https://doi.org/10.1155/2019/3191454.
[4] P. Wangchuk, K. Yeshi, K. Ugyen, J. Dorji, K. Wangdi, Samten, P. Tshering and A.S. Nugraha, Water-based therapies of bhutan: current practices and the recorded clinical evidence of balneotherapy. *Water*, 13 (2021) 9. https://doi.org/10.3390/w13010009.

[5] M.F. Hochella, S.K. Lower, P.A. Maurice, R.L. Penn, N. Sahai, D.L. Sparks, and B.S. Twining, Nanominerals, mineral nanoparticles, and earth systems. *Science*, 319 (2008) 1631-1635. https://doi.org/10.1126/science.1141134
[6] Y. Lv, D. Li, R. Liu, and Y. He, The progress and application of hot spring hydrotherapy in medical fields: A narrative review. Complement. *Ther. Med.*, 96 (2026) 103312. https://doi.org/10.1016/j.ctim.2025.103312.
[7] R. Angel, and P. Thoits, The impact of culture on the cognitive structure of illness. *Cult. Med. Psychiatry* 11 (1987) 465-494. https://doi.org/10.1007/BF00048494.
[8] C. Protano, M. Vitali, A. De Giorgi, D. Marotta, S. Crucianelli, and M. Fontana, Balneotherapy using thermal mineral water baths and dermatological diseases: a systematic review. *Int. J. Biometeorol.*, 68 (2024) 1005-1013. https://doi.org/10.1007/s00484-024-02649-x.
[9] M.A.K. Shakhatreh, J.H. Jacob, E.I. Hussein, M.M. Masadeh, S.M. Obeidat, A.S.F. Juhmani and M.A.Abd Al-Razaq, Microbiological analysis, antimicrobial activity, and heavy-metals content of Jordanian Ma'in hot-springs water. *J. Infect. Public Health*, 10 (2017) 789-793. https:doi.org/10.1016/j.jiph.2017.01.010.
[10] S. Vihodceva, Antibacterial activity of positively and negatively charged hematite (α-Fe2O3) nanoparticles to escherichia coli, staphylococcus aureus and vibrio fischeri. *Nanomater.*, 11 (2021) 652. https://doi.org/10.3390/nano11030652.
[11] M. Hosseini, S. Shakibfar and T. Saki, Engineering and process optimization of a novel Ag-assisted separation system using a naphthalene-based functional ionic liquid for the removal of organic dyes. *Ind. Eng. Chem. Res.*, 65 (2026) 8946-8961. https://doi.org/10.1021/acs.iecr.5c05326.
[12] E. Tahmasebi, M. Hosseini, M.M. Alemnezhad, F. Omidali, R. Geravand, and P.G. Kargar, Development of a sustainable magnetized bio-nano adsorbent from tomato residues for removal of Ni (II) ion from dairy effluents: Kinetics, thermodynamics, and practical applicability. *Next Mater.*, 11 (2026) 101770. https://doi.org/10.1016/j.nxmate.2026.101770
[13] E. Khalili Senobari, P.G. Kargar, M. Hosseini, and R.S. Zabibah, Pectin-chitosan-coated Fe_3O_4 nanocomposite for sustainable analysis of thymol as a food sample using MDµ-SPE. *Food Biprocess Technol.*, 19 (2026) 160. https://doi.org/10.1007/s11947-026-04245-w.
[14] M.M. Alemnezhad, M. Hosseini and M. Panahimehr, Green corrosion protection of copper in chloride media with Calystegia sepium extract using electrochemical and GC-MS/MS analyses. *Sci. Rep.*, 16 (2026) 11267. https://doi.org/10.1038/s41598-026-41526-y.
[15] A.A. Mhmood Abodiame, Z. Abdelmuttaleb Hammood, I.M. Turki, G.J. Shabaa, m. hosseini and E.A. Azooz, Green synergy: a novel deep eutectic solvent in eco-friendly air-assisted solidified floating drop microextraction for ultrasensitive lead determination. *Anal. Methods*, 18 (2026) 1304-1315. https://doi.org/10.1039/D5AY01963J.
[16] M. Hosseini and E.A. Azooz, Synthesis, characterization and application of N-methylpyrrolidinium Bisulfate ([Mpyr][HSO4]) as an efficient acidic ionic liquid catalyst for triglyceride oils interesterification. *Iran. J. Anal. Chem.*, 12 (2026) 1-11. https://doi.org/10.30473/ijac.2026.77090.1336.
[17] M. Hosseini and K. Gallardo, A novel system based on a task-specific pyrrolinium-based ionic liquid and homogeneous in situ solvent formation microextraction for the determination of sertraline in real water and urine samples. *New J. Chem.*, 49 (2025) 13772-13784. https://doi.org/10.1039/D5NJ01661D.
[18] M. Hosseini, S. Shakibafar and T. Saki, Application of deep eutectic solvents with dual function as reaction medium and catalyst for the green synthesis of azoarene and azoxyarene derivatives. *Iran. J. Anal. Chem.*, 12 (2025) 88-99. https://doi.org/10.30473/IJAC.2025.76239.1328.
[19] M. Hosseini and E.A. Azooz, Bio-inspired ionic liquid design: An advanced and environmentally friendly microextraction method for the selective separation and precise quantification of gallic acid in complex plant-derived matrices. *J. Chromatogr. B*, 1268 (2026) 124859. https://doi.org/10.1016/j.jchromb.2025.124859.
[20] M. Hosseini, A green and engineered magnetic ionic liquid system for selective extraction and trace determination of thorium in industrial and environmental samples. *Anal. Sci.*, 41 (2025) 1531-1546. https://doi.org/10.1007/s44211-025-00820-x.
[21] M. Hosseini, A. Rezaei, S.M. Koshfetrat and M.M. Alemnezhad, Detoxification of dairy industry effluent from toxic metal ions: Preparation and characterization of a magnetized adsorbent derived from agricultural residues. *Toxicol. Environ. Chem.*, 107 (2025) 98-134.

https://doi.org/10.1080/02772248.2024.2448961.

[22] M. Hosseini, R. Castillo and M. Soleymani, A novel magnetic-assisted ionic liquid-based microextraction method (MA-ILBME): Specific design system for sensitive spectrophotometric analysis of paracetamol as a pharmaceutical pollutant in environmental samples. *Talanta*, 286 (2025) 127486. https://doi.org/10.1016/j.talanta.2024.127486.

[23] S.C. Toh, S.S. Leong, S. Lihan, A.H. Lahuri, S.R. Khairul and S.S.O. Al Edrus, Identification and evaluation of thermophilic bacteria isolated from Malaysian hot springs with potential for plastic polyvinyl chloride degradation. World *J. Microbiol. Biotechnol.*, 42 (2026) 113. https://doi.org/10.1007/s11274-026-04875-4.

[24] M.A.K. Shakhatreh, J.H. Jacob, E.I. Hussein, M.M. Masadeh, S.M. Obeidat, A..F. Juhmani, and M.A. A. Al-razaq, Microbiological analysis, antimicrobial activity, and heavy-metals content of Jordanian Ma'in hot-springs water. *J. Infect. Public Health*, 10 (2017) 789-793. https://doi.org/10.1016/j.jiph.2017.01.010.

[25] X. Zhong, Z. Di, Y. Xu, Q. Liang, K. Feng, Y. Zhang, L. Di, and R. Wang, Mineral medicine: from traditional drugs to multifunctional delivery systems. *Chin. Med.*, 17 (2022) 21. https://doi.org/10.1186/s13020-022-00577-9.

[26] A. Latifi, M. Salami, E. Kazemirad, and M. Soleimani, Isolation and identification of free-living amoeba from the hot springs and beaches of the Caspian Sea. *Parasite Epidemiol. Control*, 10 (2020) e00151. https://doi.org/10.1016/j.parepi.2020.e00151.

[27] F. Heidari, H. Riahi, M. Yosefzadi, and Z. Shariatmadari, Morphological and phylogenetic diversity of cyanobacteria in four hot springs of Iran. *Iran. J. Botany*, 19 (2013) 161-172. http://dx.doi.org/10.22092/ijb.2013.4152.

[28] J. Nouraliee, S. Porkhial, M. Mohammadzadeh-Moghaddam, S. Mirzaei, D. Ebrahimi, M.R. Rahmani, Investigation of density contrasts and geologic structures of hot springs in the Markazi Province of Iran using the gravity method. *Russ. Geol. Geophys.*, 56 (2015) 1791-1800. https://doi.org/10.1016/j.rgg.2015.11.011.

[29] M. Balouiri, M. Sadiki, and S.K. Ibnsouda, Methods for in vitro evaluating antimicrobial activity: A review. *J. Pharm. Anal.*, 6 (2016) 71-79. https://doi.org/10.1016/j.jpha.2015.11.005

[30] D. Paredes, C. Ortiz, and R. Torres, Synthesis, characterization, and evaluation of antibacterial effect of Ag nanoparticles against Escherichia coli O157: H7 and methicillin-resistant Staphylococcus aureus (MRSA). *Int. J. Nanomed.*, 9 (2014) 1717. https://doi.org/10.2147/IJN.S57156.

[31] B. Lesiak, N. Rangam, P. Jiricek, I. Gordeev, J. Tóth, L. Kövér, M. Mohai, and P. Borowicz, Surface study of Fe3O4 nanoparticles functionalized with biocompatible adsorbed molecules. *Front. Chem.*, 7 (2019) 642. https://doi.org/10.3389/fchem.2019.00642.

[32] D. Mishra, R. Arora, S. Lahiri, S.S. Amritphale, and N. Chandra, Synthesis and characterization of iron oxide nanoparticles by solvothermal method. *Prot. Met. Phys. Chem. Surf.*, 50 (2014) 628-631. https://doi.org/10.1134/S2070205114050128.

[33] M.K. Hossain, A. Mishra, A. Tiwari, B. Pant, S.C. Dey, A. Tiwari, O. Saha, M.M. Rahaman, Y.R. Shukla, A. Tiwari, M. Ashaduzzaman, Thermally induced Fe_2O_3 spikes decorated Ag/Fe2O3 nanocomposite fabrication for anti-bacterial and anti-cancer activities. *SN Appl. Sci.*, 5 (2023) 339. https://doi.org/10.1007/s42452-023-05599-y.

[34] M.A. Vargas, J.E. Diosa, and E. Mosquera, Data on study of hematite nanoparticles obtained from Iron (III) oxide by the Pechini method. *Data Brief.*, 25 (2019) 104183. https://doi.org/10.1021/ef502494d.

[35] M. Mohammadi, A. Khazaei, A. Rezaei, Z. Huajun, and S. Xuwei, Ionic-liquid-modified carbon quantum dots as a support for the immobilization of tungstate ions (WO_4^{2-}): Heterogeneous nanocatalysts for the oxidation of alcohols in water. *ACS Sustain. Chem. Eng.*, 7 (2019) 5283-5291. https://doi.org/org/doi/abs/10.1021/acssuschemeng.8b06279.

[36] M. Mohammadi, A. Rezaei, A. Khazaei, S. Xuwei, and Z. Huajun, Targeted development of sustainable green catalysts for oxidation of alcohols via tungstate-decorated multifunctional amphiphilic carbon quantum dots. *ACS Appl. Mater. Interfaces*, 11 (2019) 33194-33206. https://doi.org/10.1021/acsami.9b07961.

[37] L. Hadian-Dehkordi, A. rezaei, A. Ramezani, M. Jaymanid, H. Samadian, L. Zheng, X. Deng, and H. Zheng, Amphiphilic carbon quantum dots as a bridge to a pseudohomogeneous catalyst for selective oxidative cracking of alkenes to aldehydes: A nonmetallic oxidation system. *ACS Appl. Mater. Interfaces*, 12 (2020) 31360-31371. https://doi.org/10.1021/acsami.0c05025.

[38] A. Rezaei, L. Hadian Dehkordi, H. Samadian, M. Jaymand, H. Targhan, A. Ramezani, H. Adibi, X. Deng, and H. Zheng,

Pseudohomogeneous metallic catalyst based on tungstate-decorated amphiphilic carbon quantum dots for selective oxidative scission of alkenes to aldehyde. *Sci. Rep.*, 11 (2021) 1-13. https://doi.org/10.1038/s41598-021-83863-0.

[39] Y.x. Hou, H. Abdullah, D.H. Kuo, S.J. Leu, N. S. Gultom, and and C.H. Su, A comparison study of SiO_2/nano metal oxide composite sphere for antibacterial application. *Compos. Part B: Eng.*, 133 (2018) 166-176. https://doi.org/10.1016/j.compositesb.2017.09.021.

[40] S.C. Londono, H.E. Hartnett, and B. Williams, Antibacterial activity of aluminum in clay from the Colombian Amazon. *Environ. Sci. Technol.*, 51 (2017) 2401-2408. https://doi.org/10.1021/acs.est.6b04670.

[41] B. Lyu, K. Luo, D. Gao, Y. Wang, and J. Ma, Synergistic effect of layered double hydroxide and montmorillonite: Towards super-efficient fireproofing of leather. *Appl. Clay Sci.*, 212 (2021) 106215. https://doi.org/10.1016/j.clay.2021.106215.

[42] D. Schwertfeger, J.R. Velicogna, A.H. Jesmer, S. Saatcioglu, H. McShane, R.P. Scroggins and J.I. Princz, Extracting metallic nanoparticles from soils for quantitative analysis: method development using engineered silver nanoparticles and SP-ICP-MS. *Anal. Chem.*, 89 (2017) 2505-2513. https://doi.org/10.1021/acs.analchem.6b04668.

[43] I.C. Regelink, L. Weng, and W.H. van Riemsdijk, The contribution of organic and mineral colloidal nanoparticles to element transport in a podzol soil. *Appl. Geochem.*, 26 (2011) S241-S244. https://doi.org/10.1016/j.apgeochem.2011.03.114.

[44] A. Shavandi, P. Saeedi, M.A. Ali, and E. Jalalvandi, Functional Polysaccharides for Biomedical Applications, (2019) 267-304 (1st Edition, Elsevier).

[45] V.K. Sharma, J. Filip, R. Zboril, and R.S. Varma, Natural inorganic nanoparticles-formation, fate, and toxicity in the environment. *Chem. Soc. Rev.*, 44 (2015) 8410-8423. https://doi.org/10.1039/C5CS00236B.

[46] S. Bhandari, and T.K. Nailwal, Recent Advancements in Microbial Diversity, (2020) 251-288, (1st Edition, Elsevier).

[47] N. Baheiraei, H. Eyni, B. Bakhshi, R. Najafloo, and N. Rabiee, Effects of strontium ions with potential antibacterial activity on in vivo bone regeneration. *Sci. Rep.*, 11 (2021) 1-9. https://doi.org/10.1038/s41598-021-88058-1.

[48] Y.P. Li, I. Ben Fekih, E.C. Fru, and G. Wang, Antimicrobial activity of metals and metalloids. *Annu. Rev. Microbiol.*, 75 (2021) 175-197. https://doi.org/10.1146/annurev-micro-032921-123231.

[49] V. Prado, R. Vidal, and C. Durán, Aplicación de la capacidad bactericida del cobre en la práctica médica. *Rev. Med. Chile*, 140 (2012) 1325-1332. http://dx.doi.org/10.4067/S0034-98872012001000014.

[50] A. Anastasiou, M. Nerantzaki, E. Gounari, M.S. Duggal, P.V. Giannoudis, A. Jha, and D. Bikiaris, Antibacterial properties and regenerative potential of Sr^{2+} and Ce^{3+} doped fluorapatites; a potential solution for peri-implantitis. *Sci. Rep.*, 9 (2019) 1-11. https://doi.org/10.1038/s41598-019-50916-4.

DOI: 10.30473/IJAC.2026.78061.1346

بررسی تجزیه‌ایی یکپارچه نانوذرات معدنی موجود در آب چشمه آب گرم بکتر با تأکید بر عملکرد ضدباکتریایی

رستم جمالی اسلامی[۱]، مهدی حسینی[*۲]

۱. دبیرستان خوارزمی شهرستان سنقر کلیایی، سنقر، کرمانشاه، ایران.

۲. گروه شیمی، دانشکده علوم پایه، استادیار شیمی تجزیه–دانشگاه آیت‌ا... بروجردی، بروجرد، ایران.

* E-mail: Hosseini.mih@gmail.com; Hosseini.mehdi@abru.ac.ir

تاریخ دریافت: ۲۶ اردیبهشت ۱۴۰۴ **تاریخ پذیرش:** ۲۸ تیر ۱۴۰۴

چکیده

چشمه‌های آب گرم، سامانه‌های زمین‌گرمایی طبیعی هستند که با مواد معدنی محلول و ذرات در مقیاس نانو و میکرو غنی شده‌اند و این ویژگی می‌تواند در خواص درمانی سنتی آن‌ها نقش داشته باشد. در این مطالعه، برای نخستین‌بار نانوذرات معدنی (MNPs) از آب چشمه آب گرم بکتر واقع در غرب ایران جدا شده و ویژگی‌های فیزیکوشیمیایی آن‌ها همراه با فعالیت ضدباکتریایی مورد بررسی قرار گرفت. تحلیل‌های ساختاری به‌وسیله طیف‌سنج مادون قرمز تبدیل فوریه (FTIR)، پراش پرتو ایکس (XRD)، فلورسانس پرتو ایکس (XRF)، طیف‌سنجی جرمی پلاسمای جفت‌شده القایی (ICP-MS) و آنالیز گرماسنجی (TGA) نشان داد که این ذرات عمدتاً از فازهای سیلیکاتی و اکسیدهای فلزی تشکیل شده‌اند و دارای مقادیر بالایی از (07/54%) SiO2، (20/15%) Al2O3، (19/7%) CaO و Fe2O3 A (۵/۴۵٪) هستند. همچنین نتایج ICP-MS وجود مقادیر قابل توجهی از عناصر کم‌مقدار و فلزات سنگین از جمله استرانسیوم (ppm 9/685)، وانادیوم (ppm 139)، کروم ((ppm 105)، روی (ppm 85) و مس (ppm 63) را تایید کرد. انالیز پراش اشعه ایکس نشان داد که میانگین اندازه ذرات بلوری در حدود ۴۹/۷ نانومتر می باشد. فعالیت ضدباکتریایی نانوذرات خام (غیرحرارت‌دیده) و حرارت‌دیده در برابر باکتری‌های Staphylococcus aureus ATCC 43300 و Pseudomonas aeruginosa با استفاده از آزمون نفوذ دیسک و تعیین حداقل غلظت مهارکننده (MIC) ارزیابی شد. قطر ناحیه عدم رشد برای نانوذرات غیرحرارت‌دیده در برابر باکتری P. aeruginosa به ۱۹±۰.۵ میلی‌متر رسید، در حالی‌که این مقدار برای S. aureus کمتر و برابر ۹.۳۲±۰.۱۵ میلی‌متر بود. همچنین هر دو نوع نانوذره حرارت‌دیده و غیرحرارت‌دیده، حداقل غلظت مهارکننده ۱۵۰ میکروگرم بر میلی‌لیتر را نشان دادند. نتایج به‌دست‌آمده نشان داد که نانوذرات معدنی طبیعی موجود در چشمه آب گرم بکتر دارای فعالیت ضدباکتریایی قابل توجهی هستند و می‌توانند نقش بالقوه‌ای در توجیه اثرات درمانی سامانه‌های زمین‌گرمایی و کاربردهای زیست‌پزشکی داشته باشند.

کلیدواژه‌ها

نانوذرات معدنی طبیعی، تعیین مقدار ناچیز عناصر، آب گرم چشمه، آنالیز نانومواد، مهار باکتریایی.

DOI: 10.30473/IJAC.2026.78061.1346